
RECURSIVE NEAREST NEIGHBOR CO-KRIGING MODELS FOR BIG MULTIPLE FIDELITY SPATIAL DATA SETS

A PREPRINT

Si Cheng¹, Bledar A. Konomi ^{*1}, Georgios Karagiannis², and Emily L. Kang¹

¹Division of Statistics and Data Sciences, Department of Mathematical Sciences, University of Cincinnati, USA

²Mathematical Sciences, Durham University, UK

February 28, 2023

ABSTRACT

Large datasets are daily gathered from different remote sensing platforms and statistical models are usually used to combine them by accounting for spatially varying bias corrections. The statistical inference of these models is usually based on Markov chain Monte Carlo (MCMC) samplers which involve updating a high-dimensional random effect vector and hence present slow mixing and convergence. To overcome this and enable fast inference in big spatial data problems, we propose the recursive nearest neighbor co-kriging (RNNC) model and use it as a framework which allows us to develop two computationally efficient inferential procedures: a) the collapsed RNNC that reduces the posterior sampling space by integrating out the latent processes, and b) the conjugate RNNC which is an MCMC free inference that significantly reduces the computational time without sacrificing prediction accuracy. The good computational and predictive performance of our proposed algorithms are demonstrated on benchmark examples and the analysis of the High-resolution Infrared Radiation Sounder data gathered from two NOAA polar orbiting satellites in which we managed to reduce the computational time from multiple hours to just a few minutes.

Keywords: Recursive Co-kriging Model, Nearest neighbor Gaussian process, Remote Sensing

1 Introduction

Global geophysical information is measured daily by numerous satellite sensors. Due to aging and exposure to the harsh environment of space the satellite sensors degrades over time causing a decrease on performance reliability. This decrease on performance may result in inaccuracy of the data measurements (Goldberg, 2011). In addition, newer satellites with technologically more advanced sensors provide information of higher fidelity than older sensors. These discrepancies in sensors performances have created the need to develop efficient methods to analyse daily global remote sensing measurements with varying fidelity. Our work in this manuscript is motivated by data products from the high-resolution infrared radiation sounder (HIRS) which provides daily hundred of thousands of measurements from multiple satellite platforms.

*Corresponding author: Bledar A. Konomi (alex.konomi@uc.edu)

Multiple methods in remote sensing have been developed to assess satellite sensor performance and consistency (Chander et al., 2013; Xiong et al., 2010; National Research Council, 2004). These methods do not account for spatial correlation and oversimplify the relationship between sensors. On the other hand statistical methods to analyse these data sets and accounting for spatial correlation are also challenging due to the multifidelity presence as well as the size and computationally intensive procedures. Nguyen et al. (2012, 2017) have proposed data fusion techniques to model multivariate spatial data at potentially different spatial resolutions based on fixed ranked kriging (Cressie and Johannesson, 2008). The accuracy of this approach relies on the number of basis functions and can only capture large scale variation of the covariance function. When the data sets are dense, strongly correlated, and the noise effect is sufficiently small, the low rank kriging techniques have difficulty to account for small scale variation (Stein, 2014).

Autoregressive co-kriging models (Kennedy and O’Hagan, 2000; Qian et al., 2005; Le Gratiet, 2013), which have been originally built for computer simulation problems, can also be used for the analysis of multiple fidelity remote sensing observations when they have spatially nested structure. Konomi and Karagiannis (2021); Ma et al. (2022) relaxed the nested design requirements by using imputation ideas and properly augmenting the data. However, the aforesaid methods rely on Gaussian process models and are computationally impossible for big data problems. For cases when the observed space can be expressed as a tensor product Konomi et al. (2023) uses a separable covariance function within the co-kriging model to improve the computational efficiency. For more general cases of the observed space, Cheng et al. (2021) proposed the nearest neighbour co-kriging Gaussian process (NNCGP) which embeds nearest neighbor Gaussian process (NNGP; Datta et al., 2016) into an autoregressive co-kriging model to make computations possible. The proposed NNCGP uses imputation ideas into the latent variables to construct a nested reference set of multiple NNGP levels. Despite the fact that the NNCGP makes the analysis of big multi-fidelity data sets computationally possible, its computational speed depends on an expensive iterative procedure which makes it impractical for analysing daily large data sets.

To overcome the iterative MCMC procedure, we propose a recursive formulation based on the latent variable of the NNCGP model following similar ideas with Le Gratiet and Garnier (2014) who proposed the recursive formulation directly in the observations. Based on this new formulation, which we call recursive nearest neighbors co-kriging (RNNC), we are able to build a nearest neighbors co-kriging model with T levels by building T conditionally independent NNGPs. This enables the development of two alternative inferential procedures which aim to reduce high-dimensional parametric space, improve convergence, and reduce computational time in comparison to the NNCGP. Both proposed procedures are able to address applications for large non-nested and irregular spatial data sets from different platforms and with varying quality. In the first proposed alternative procedure that we call Collapsed RNNC, we reduce the MCMC posterior sampling space by integrating out the spatial latent variables. Based on the RNNC, we propose an MCMC free procedure to achieve Bayesian inference. We build an algorithm which sequentially decomposes the parametric space into conditionally independent parts for every fidelity level so that we are able to use a combination of closed form conditional means and K-fold optimization method. Each sequential step can be viewed as collapsed NNGP (Finley et al., 2019a) where the bases component of the mean is determined at the previous step. We name this second inferential procedure conjugate RNNC. We note that the MCMC free procedure proposed in (Finley et al.,

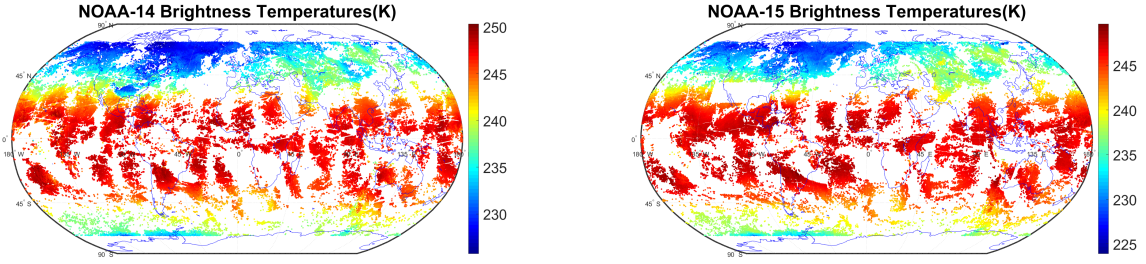
2019a) cannot be applied directly in the NNCGP because the computational complexity of the K -fold cross-validation method depends on the dimension of the parametric space. Based on our simulation study and the analysis of the HERS data sets, we show that the proposed conjugate RNNC procedure reduces the computational time notably without significantly sacrificing prediction accuracy over the existing NNCGP approach.

The layout of the paper is as follows. In Section 2, we introduce the high-resolution infrared radiation sounder data studied in this work. In Section 3, we review the autoregressive co-kriging and NNCGP model. In Section 4, we introduce the proposed RNNC model. In Section 4.1, we integrate out the latent variables from the model and design an MCMC algorithm for this model. In Section 4.2, we design an MCMC free approach tailored to the proposed RNNC model that facilitates parametric and predictive inference. In Section 6, we investigate the performance of the proposed procedure on a simulation example. In Section 7, we implement the proposed method for the analysis of data sets from two satellites, NOAA-14 and NOAA-15. Finally, we conclude in Section 8.

2 High-resolution Infrared Radiation Sounder Data

Satellite soundings have been providing measurements of the Earth’s atmosphere, oceans, land, and ice since the 1970s to support the study of global climate system dynamics. Long term observations from past and current environmental satellites are widely used in developing climate data records (CDR) (National Research Council, 2004). HIRS mission objectives include observations of atmospheric temperature, water vapor, specific humidity, sea surface temperature, cloud cover, and total column ozone. The HIRS instrument is comprised of twenty channels, including twelve longwave channels, seven shortwave channels, and one visible channel. The dataset being considered in this study is limb-corrected HIRS swath data as brightness temperatures (Jackson et al., 2003). The data is stored as daily files, where each daily file records approximately 120,000 geolocated observations. The current archive includes data from NOAA-5 through NOAA-17 along with Metop-02, covering the time period of 1978-2017. In all, this data archive is more than 2 TB, with an average daily file size of about 82 MB. The HIRS CRD faces some common challenges regarding the consistency and accuracy over time, due to degradation of sensors and intersatellite discrepancies. Furthermore, there is missing information caused by atmospheric conditions such as thick cloud cover.

We examine HIRS Channel 5 observations from a single day, March 1, 2001, as illustrated in Figure 1. On this day, we may exploit a period of temporal overlap in the NOAA POES series where two satellites captured measurements: NOAA-14 and NOAA-15. The HIRS sensors on these two satellites have similar technical designs which allow us to ignore the spectral and spatial footprint differences. NOAA-14 became operational in December 1994 while NOAA-15 became operational in October 1998. The spatial resolution footprint for both satellites is approximately 10 km at nadir. Given the sensor age difference, it is reasonable to consider that the instruments on-board NOAA-15 are in better condition than those of NOAA-14. Therefore, we treat observations from NOAA-14 as a dataset of low fidelity level, and those from NOAA-15 as a dataset of high fidelity level.



(a) Observations of NOAA 14

(b) Training data of NOAA 15

Figure 1: NOAA-14 Brightness Temperatures observation data-set, NOAA-15 Brightness Temperatures training data-set for Channel 5 on March 1, 2001.

3 Nearest Neighbor Co-kriging Gaussian Process

Let $y_t(s)$ denote the output function at the spatial location s at fidelity level $t = 1, \dots, T$ in a system with fidelity T levels. The fidelity level index t runs from the least accurate to the most accurate one. Let $z_t(s)$ denote the observed output at location s . We specify an autoregressive co-kriging model as

$$\begin{aligned}
z_t(\mathbf{s}) &= y_t(\mathbf{s}) + \epsilon_t, \\
y_t(\mathbf{s}) &= \zeta_{t-1}(\mathbf{s})y_{t-1}(\mathbf{s}) + \delta_t(\mathbf{s}), \\
\delta_t(\mathbf{s}) &= \mathbf{h}_t^T(\mathbf{s})\boldsymbol{\beta}_t + w_t(\mathbf{s}),
\end{aligned} \tag{3.1}$$

where $z_t(\mathbf{s})$ is contaminated by additive random noise $\epsilon_t \sim N(0, \tau_t^2)$ for $t = 2, \dots, T$, and $y_1(\mathbf{s}) = \mathbf{h}_1^T(\mathbf{s})\boldsymbol{\beta}_1 + w_1(\mathbf{s})$ is the noiseless output. Here, $\zeta_{t-1}(\mathbf{s})$ and $\delta_t(\mathbf{s})$ represent the scale and additive discrepancies between systems with fidelity levels t and $t-1$, $\mathbf{h}_t(\cdot)$ is a design matrix, and $\boldsymbol{\beta}_t$ is a vector of coefficients at fidelity level t . We model the latent function $w_t(\mathbf{s})$ as a Gaussian processes, mutually independent for different t ; i.e. $w_t(\cdot) \sim GP(0, C_t(\cdot, \cdot; \boldsymbol{\theta}_t))$ where $C_t(\cdot, \cdot; \boldsymbol{\theta}_t)$ is a cross-covariance function with covariance parameters $\boldsymbol{\theta}_t$ at fidelity level t . Any well defined covariance function can be used $C_t(\mathbf{s}, \mathbf{s}' | \boldsymbol{\theta}_t) = \sigma_t^2 R(\mathbf{s}, \mathbf{s}' | \boldsymbol{\phi}_t)$, where $\boldsymbol{\theta}_t = \{\sigma_t^2, \boldsymbol{\phi}_t\}$.

This indicates that discrepancy term $\delta_t(\mathbf{s})$ given $\mathbf{h}_t^T(\mathbf{s})\boldsymbol{\beta}_t$ is a Gaussian process. The unknown scale discrepancy function $\zeta_{t-1}(s)$ is modeled as a basis expansion $\zeta_{t-1}(\mathbf{s} | \boldsymbol{\gamma}_{t-1}) = \mathbf{g}_{t-1}(\mathbf{s})^T \boldsymbol{\gamma}_{t-1}$ (usually low degree), where $\mathbf{g}_t(\mathbf{s})$ is a vector of polynomial basis functions and $\{\boldsymbol{\gamma}_{t-1}\}$ is a vector of random coefficients, for $t = 2, \dots, T$.

Let us assume the system is observed at n_t locations at fidelity level t . Let $\mathbf{S}_t = \{s_{t,1}, \dots, s_{t,n_t}\}$ be the set of n_t observed locations, let $\mathbf{w}_t = w_t(\mathbf{S}_t) = \{w_t(s_{t,1}), \dots, w_t(s_{t,n_t})\}$ the latent spatial random effect vector at fidelity level t , and let $\mathbf{Z}_t = z_t(\mathbf{S}_t) = \{z_t(s_{t,1}), \dots, z_t(s_{t,n_t})\}$ represent the observed output at fidelity level t . If data $\{\mathbf{Z}_t\}$ are observed in non-nested locations across the fidelity levels, the calculation of the likelihood requires $\mathcal{O}((\sum_{t=1}^T n_t)^3)$ flops to invert the covariance matrix of the observations (which we denote by $\boldsymbol{\Lambda}$) and additional $\mathcal{O}((\sum_{t=1}^T n_t)^2)$ memory

to store it as explained in Konomi and Karagiannis (2021). To reduce the computational complexity, Cheng et al. (2021) proposed NNCGP which assigns independent nested NNGP priors within a nested reference set. For Bayesian inference, Cheng et al. (2021) proposed a Gibbs sampler which is able to take advantage of the nearest neighbour structure at each level. However, this sampler is based on updating a conditionally independent high dimensional latent variable which could cause slow convergence and high autocorrelation (Liu et al., 1994). The slow convergence can significantly increase the number of the Gibbs sampler iterations I and has an overall computational cost of $\mathcal{O}(I \times \tilde{n}_1 m^2)$ flops. For a fixed computational budget, the produced Monte Carlo estimates may be sensitive to the initial values of the MCMC sampler. Despite reducing the computational complexity to linear for every MCMC iteration, the number of the iterations can significantly increase computational cost. This simple observation makes the NNCGP too expensive for the vast majority of real remote sensing applications.

4 Recursive Nearest Neighbor Co-kriging Model

Improvement of MCMC convergence can be achieved by integrating out the latent variable $\mathbf{w} = (\mathbf{w}_1, \dots, \mathbf{w}_S)$ from the Bayesian hierarchical NNCGP model which allows the reduction of the dimensionality of the involved posterior distributions. However, integrating out the latent variables \mathbf{w} in the NNCGP model is not infeasible for non-nested observations. This is because the posterior distribution of latent variable of the lower fidelity is affected by the likelihood of higher fidelity. To make possible the integration of latent variables \mathbf{w} , and relax the dependencies of the latent variables, we propose a recursive formulation for the co-kriging model by using ideas from (Le Gratiet and Garnier, 2014) and then coupling it with strategies similar to Finley et al. (2019b) with purpose to integrate out the latent variable \mathbf{w} . Precisely, our proposed recursive nearest neighbors co-kriging (RNNC) has the following hierarchical structure:

$$\begin{aligned} z_t(\mathbf{s}) &= y_t(\mathbf{s}) + \epsilon_t \\ y_t(\mathbf{s}) &= \zeta_{t-1}(\mathbf{s})\hat{y}_{t-1}(\mathbf{s}) + \delta_t(\mathbf{s}), \\ \delta_t(\mathbf{s}) &= \mathbf{h}_t^T(\mathbf{s})\boldsymbol{\beta}_t + w_t(\mathbf{s}), \end{aligned} \tag{4.1}$$

where $\delta_t(\mathbf{s})$ is a Gaussian process as before and $\hat{y}_{t-1}(\mathbf{s})$ is a Gaussian process with distribution $[\hat{y}_{t-1}(\mathbf{s})|\mathbf{Z}_{t-1}, \hat{y}^{t-2}(\mathbf{s}), \boldsymbol{\theta}_{t-1}]$. Basically, we express $y_t(\mathbf{s})$ (the Gaussian process modeling the response at level t) as a function of the Gaussian process $y_{t-1}(x)$ conditioned by the values $\mathbf{Z}^{(t-1)} = (\mathbf{Z}_1, \dots, \mathbf{Z}_{t-1})$. For computational efficiency, we assume NNGP independent priors for $w_t(\mathbf{s})$, $t = 1, \dots, T$. Based on the NNGP priors, the conditional distribution can be computed for all types of reference sets. So, based on the recursive representation we can relax the nested condition on the NNCGP nested reference set.

$$\hat{y}_{t-1}(\mathbf{s})| \cdot \sim N(\zeta_{t-2}\hat{y}_{t-2}(\mathbf{s}) + \mathbf{h}_{t-1}^T(\mathbf{s})\boldsymbol{\beta}_{t-1} + V_{t-1,s}\mu_{t-1,s}, V_{t-1,s}), \tag{4.2}$$

with, $\mu_{t-1,s} = V_{t-1,s}^{-1}\mathbf{B}_{t-1,s} \left[z_{t-1}(N_{t-1}(\mathbf{s})) - \mathbf{h}_{t-1}^T(N_{t-1}(\mathbf{s}))\boldsymbol{\beta}_{t-1} - \zeta_{t-2}(N_{t-1}(\mathbf{s})) \circ \hat{y}_{t-2}(N_{t-1}(\mathbf{s})) \right]$, $\mathbf{B}_{t,s} = C_{\mathbf{s},N_t(\mathbf{s})}^T C_{N_t\mathbf{s}}^{-1}$, and $V_{t,s} = C(\mathbf{s}, \mathbf{s}) - C_{\mathbf{s},N_t(\mathbf{s})}^T C_{N_t\mathbf{s}}^{-1} C_{\mathbf{s},N_t(\mathbf{s})}$.

Using the Markovian property of the co-kriging model (O’Hagan, 1998), the joint likelihood of the proposed model in (4.1) can be factorized as a product of likelihoods from different fidelity levels conditional on $\hat{y}_{t-1}(\mathbf{S}_t)$ for $t = 2, \dots, T$ and prior \mathbf{w}_t for $t = 1, \dots, T$, i.e.:

$$\begin{aligned} L(\mathbf{Z}_{1:T}|\cdot) &= p(\mathbf{Z}_1|\mathbf{w}_1, \boldsymbol{\beta}_1, \tau_1) \prod_{t=2}^T p(\mathbf{Z}_t|\mathbf{w}_t, \boldsymbol{\beta}_t, \hat{y}_{t-1}(\mathbf{S}_t), \gamma_{t-1}, \tau_t) \\ &= N(\mathbf{Z}_1|\mathbf{h}_1(\mathbf{S}_1)\boldsymbol{\beta}_1 + \mathbf{w}_1, \tau_1\mathbf{I}) \prod_{t=2}^T N(\mathbf{Z}_t|\zeta_{t-1}(\mathbf{S}_t) \circ \hat{y}_{t-1}(\mathbf{S}_t) + \mathbf{h}_t(\mathbf{S}_t)\boldsymbol{\beta}_t + \mathbf{w}_t, \tau_t\mathbf{I}), \end{aligned} \quad (4.3)$$

where \circ is the Hadamard production symbol. This representation makes it possible to integrate out the latent variable \mathbf{w}_t for $t = 1 \dots T$ independently for each fidelity level.

4.1 Collapsed Recursive Nearest Neighbor Co-kriging Model

We represent the multivariate Gaussian latent variable $\mathbf{w}_t(\mathbf{S}_t)$ as a linear model:

$$\begin{aligned} w_t(\mathbf{s}_{t,1}) &= 0 + \eta_{t,1}, \\ w_t(\mathbf{s}_{t,i}) &= a_{t,i,1}w_t(\mathbf{s}_{t,1}) + a_{t,i,2}w_t(\mathbf{s}_{t,2}) + \dots + a_{t,i,i-1}w_t(\mathbf{s}_{t,i-1}) + \eta_{t,i}, \text{ for } i = 2, \dots, n_t \end{aligned}$$

for $t = 1, \dots, T$. We set $\eta_{t,i} \sim N(0, d_{t,i,i})$ independently for all t, i , $d_{t,1,1} = \delta(w_{t,1})$ and $d_{t,i,i} = \delta(w_{t,i}|\{w_{t,j}; j < i\})$ for $i = 2, \dots, n_t$ and $t = 1, \dots, T$. In a matrix form we can write $\mathbf{w}_t(\mathbf{S}_t) = \mathbf{A}_t\mathbf{w}_t(\mathbf{S}_t) + \boldsymbol{\eta}_t$, where \mathbf{A}_t is an $n \times n$ strictly lower-triangular matrix and $\boldsymbol{\eta}_t \sim N(0, \mathbf{D})$ and \mathbf{D} is diagonal. Based on the structure of \mathbf{A}_t , we can write the covariance of each level as $\mathbf{C}_t(\boldsymbol{\theta}_t) = (\mathbf{I}_t - \mathbf{A}_t)^{-1}\mathbf{D}_t(\mathbf{I}_t - \mathbf{A}_t)^{-T}$. The NNGP prior constructs a sparse strictly lower triangular matrix \mathbf{A} with no more than m ($\ll n$) non-zero entries in each row resulting in an approximation of the covariance matrix \mathbf{C}_t . So the approximated inverse $\tilde{\mathbf{C}}_t^{-1}(\boldsymbol{\theta}_t) = (\mathbf{I}_t - \mathbf{A}_t)\mathbf{D}_t^{-1}(\mathbf{I}_t - \mathbf{A}_t)^T$ is a sparse matrix and can be computed based on $O(nm^2)$ operations.

We call the integrated version of the above model collapsed RNNC model. Specifically, after integrating out \mathbf{w}_t the proposed RNNC model can be written as:

$$\begin{aligned} z_1(\mathbf{S}_1)|\cdot &\sim N(\mathbf{h}_1^T(\mathbf{S}_1)\boldsymbol{\beta}_1, \tilde{\boldsymbol{\Lambda}}_1(\mathbf{S}_1, \boldsymbol{\theta}_1, \tau_1)), \\ z_t(\mathbf{S}_t)|\cdot &\sim N(\zeta_t(\mathbf{S}_t) \circ \hat{y}_{t-1}(\mathbf{S}_t) + \mathbf{h}_t^T(\mathbf{S}_t)\boldsymbol{\beta}_t, \tilde{\boldsymbol{\Lambda}}_t), \end{aligned} \quad (4.4)$$

for $t = 2, \dots, T$, where $\tilde{\boldsymbol{\Lambda}}_t(\boldsymbol{\theta}_t, \tau_t) = \tilde{\mathbf{C}}_t(\boldsymbol{\theta}_t) + \tau_t^2\mathbf{I} = \sigma_t^2\tilde{\mathbf{R}}_t(\boldsymbol{\phi}_t) + \tau_t^2\mathbf{I}$ is the covariance matrix of the observations, $\tilde{\mathbf{C}}_t(\boldsymbol{\theta}_t)$ is the sparse covariance matrix with parameters $\boldsymbol{\theta}_t = \{\sigma_t^2, \boldsymbol{\phi}_t\}$ and τ_t^2 is the variance of the error ϵ_t at level t . By applying Sherman-Morrison-Woodbury formula, the inverse and determinant of $\tilde{\boldsymbol{\Lambda}}$ get the computationally convenient form

$$\begin{aligned} \tilde{\boldsymbol{\Lambda}}_t^{-1} &= \tau_t^{-2}\mathbf{I} - \tau_t^{-4}(\tilde{\mathbf{C}}_t(\boldsymbol{\theta}_t)^{-1} + \tau_t^{-2}\mathbf{I})^{-1}, \\ \det(\tilde{\boldsymbol{\Lambda}}_t) &= \tau_t^{2n}\det(\tilde{\mathbf{C}}_t(\boldsymbol{\theta}_t))\det(\tilde{\mathbf{C}}_t(\boldsymbol{\theta}_t)^{-1} + \tau_t^{-2}\mathbf{I}). \end{aligned}$$

Here, $y_{t-1}(\mathbf{S}_{t-1})$ is the latent noiseless output at fidelity level $t - 1$ with a space covariance matrix defined by the nearest neighbors. To reduce the dimensionality of \hat{y} variables, for nested location $s_u \in \mathbf{S}_{t-1}$, we use an empirical

approach to estimate $\hat{y}_{t-1}(s_u)$ by $z_{t-1}(s_u)$. Based on this representation, the joint posterior distribution is approximated as:

$$p(\Theta_{1:T}|\mathbf{Z}_{1:T}) \approx p(\Theta_1)\tilde{L}(\mathbf{Z}_1|\Theta_1) \prod_{t=2}^T \int p(\Theta_t)\tilde{L}(\mathbf{Z}_t|\Theta_t, \hat{\mathbf{y}}_{t-1}(\mathbf{S}_t))\tilde{p}(\hat{\mathbf{y}}_{t-1}(\mathbf{S}_t^*)|\cdot) d\hat{\mathbf{y}}_{t-1}(\mathbf{S}_t^*), \quad (4.5)$$

where $\tilde{L}(\mathbf{Z}_t|\Theta_t, \hat{\mathbf{y}}_{t-1}(\mathbf{S}_t))$ is the approximated likelihood using the space representation and $\tilde{p}(\hat{\mathbf{y}}_{t-1}(\mathbf{S}_t^*)|\cdot)$ the nearest neighbor Gaussian process prediction at locations $\mathbf{S}_t^* = \bigcup_{i=t+1}^T \mathbf{S}_i \setminus \mathbf{S}_t = \{s_{t,1}^*, \dots, s_{t,n_t}^*\}$ as a set of knots of fidelity level t . This contains the observed locations that are not in the t^{th} level but in the higher fidelity levels. Note that the prediction probability can be excluded for cases with hierarchically nested structure for the spatial locations. For hierarchical nested structure for the spatial locations, it can be proven that the prediction distribution mean and variance of level T is the same as the mean and variance of the prediction distribution of the NNCGP. The proof is similar to Le Gratiet and Garnier (2014) where we substitute the GP priors with the NNGP priors and adding the nugget effect in each level.

By assigning independent conjugate prior $\beta_t \sim N(\boldsymbol{\mu}_{\beta_t}, \mathbf{V}_{\beta_t})$ and $\gamma_t \sim N(\boldsymbol{\mu}_{\gamma_t}, \mathbf{V}_{\gamma_t})$, the conditional distribution for parameters β_t and γ_t is:

$$\beta_t|\cdot \sim N(\mathbf{V}_{\beta_t}^* \boldsymbol{\mu}_{\beta_t}^*, \mathbf{V}_{\beta_t}^*), \quad (4.6)$$

$$\gamma_t|\cdot \sim N(\mathbf{V}_{\gamma_t}^* \boldsymbol{\mu}_{\gamma_t}^*, \mathbf{V}_{\gamma_t}^*), \quad (4.7)$$

where $\mathbf{V}_{\beta_t}^*, \boldsymbol{\mu}_{\beta_t}^*, \mathbf{V}_{\gamma_t}^*, \boldsymbol{\mu}_{\gamma_t}^*$ are give in Appendix C. The posterior density functions of $\tau_t^2, \boldsymbol{\theta}_t$ is not given in closed form because they appear in the covariance matrix $\tilde{\boldsymbol{\Lambda}}_t$. A Metropolis-Hastings (MH) algorithm targeting the distribution $p(\boldsymbol{\theta}_t, \tau_t^2|\mathbf{Z}_t, \mathbf{y}_{t-1}(\mathbf{S}_t), \beta_t)$ can be used for the Monte Carlo estimation of these parameters.

4.2 Conjugate Recursive Nearest Neighbor Co-kriging Model

Both NNCGP and collapsed RNNC models are fully Bayesian approaches which are able to provide the joint posterior distributions for multi-fidelity systems. They both rely on the MCMC inference which can be practically prohibitive when analyzing thousands or millions of spatial data sets. We design an MCMC free procedure to achieve exact Bayesian inference at a more practical time based on Finley et al. (2019a) estimation strategies. Because the computational efficiency of the estimation procedure in Finley et al. (2019a) is sensitive to the number of parameters, it cannot be applied directly to our model. We utilize the RNNC model conditionally independent posterior representation to decompose the parametric space into smaller different groups based on the fidelity levels. To make MCMC free inference possible, we re-paramterize the covariance function of the collapsed recursive co-kriging model as $\tilde{\boldsymbol{\Lambda}}_t(\boldsymbol{\theta}_t, \tilde{\tau}_t^2) = \sigma_t^2 \tilde{\boldsymbol{\Sigma}}_t$, where $\tilde{\boldsymbol{\Sigma}}_t = \tilde{\mathbf{R}}_t + \tilde{\tau}_t^2 \mathbf{I}$, $\tilde{\mathbf{R}}_t$ is the nearest-neighbor approximation correlation matrix, and $\tilde{\tau}_t^2 = \frac{\tau_t^2}{\sigma_t^2}$. To avoid the computational bottleneck due to the MCMC, we propose to make fast estimation $(\phi_t, \tilde{\tau}_t^2)$ through a cross-validation approach independently for each level as well as using the prediction means of $\mathbf{y}_{t-1}(\mathbf{S}_t)$ based on the estimated values. We estimate $\hat{y}_t(\mathbf{S}_t^*)$ by the posterior mean $\bar{y}_t(\mathbf{S}_t^*) = \mathbf{1}_{t>1}(t)\mathbf{g}_{t-1}^T(\mathbf{S}_t^*)\hat{\mathbf{y}}_{t-1}(\mathbf{S}_t^*) + \mathbf{h}_t^T(\mathbf{S}_t^*)\hat{\boldsymbol{\beta}}_t + V_{t, \mathbf{S}_t^*} \mu_{t, \mathbf{S}_t^*}$. In the case that we have some points nested, $y_t(s_u)$ for a location $s_u \in \mathbf{S}_{t-1}$ is estimated with an empirical approach $\bar{y}_{t-1}(s_u)$ as $z_{t-1}(s_u)$ and its variance is equal to the variance of the nugget effect.

Algorithm 1 The Algorithm steps for the MCMC free conjugate RNNC procedure. MCMC free posterior sampling for multi-fidelity level system with T levels.

step 1 Start from fidelity level 1($t = 1$), construct a set L_t that contains l_t numbers of candidates of parameters ϕ_t and $\tilde{\tau}_t^2$.

step 2 Choose a $(\phi_t, \tilde{\tau}_t^2)$ from L_t . Split the data set of fidelity level t into K folds.

step 3 Remove k^{th} fold of data set \mathbf{S}_t , denote as $\mathbf{S}_{t,k}$, then estimate $\sigma_t^2|\mathbf{Z}_t, \hat{y}_{t-1}(\mathbf{S}_t)$ by posterior mean $\hat{\sigma}_t^2 = \frac{b_t^*}{a_t^*-1}$ by (4.11),(D.5). Estimate $\beta_t|\sigma_t^2, \mathbf{Z}_t, \hat{y}_{t-1}(\mathbf{S}_t)$ by posterior mean $\hat{\beta}_t = \tilde{\mathbf{V}}_{\beta_t} \tilde{\boldsymbol{\mu}}_{\beta_t}$ (4.10),(D.4). Estimate $\gamma_{t-1}|\beta_t, \sigma_t^2, \mathbf{Z}_t, \hat{y}_{t-1}(\mathbf{S}_t)$ by posterior mean $\hat{\gamma}_{t-1} = \tilde{\mathbf{V}}_{\gamma_{t-1}} \tilde{\boldsymbol{\mu}}_{\gamma_{t-1}}$ (4.9).

step 4 Predict test data set $z_t(\mathbf{S}_{t,k})$ by posterior mean

$$\hat{z}_t(\mathbf{S}_{t,k}) = \mathbf{1}_{t>1}(t) \mathbf{g}_{t-1}^T(\mathbf{S}_{t,k}) \hat{\gamma}_{t-1} \hat{y}_{t-1}(\mathbf{S}_{t,k}) + \mathbf{h}_t^T(\mathbf{S}_{t,k}) \hat{\beta}_t + V_{t,\mathbf{S}_{t,k}} \mu_{t,\mathbf{S}_{t,k}}.$$

step 5 Repeat steps 3-4 over all K folds, calculate the average root mean square prediction error(RMSPE) by

$$\text{RMSPE} = \frac{\sum_{k=1}^K \left[\sum_{\mathbf{s}=\mathbf{S}_{t,k}} (z_t(\mathbf{s}) - \hat{z}_t(\mathbf{s}))^2 / n_k \right]}{K}.$$

step 6 Repeats steps 2-5 over all values in candidate set L_t , choose the value of $\hat{\phi}_t$ and $\hat{\tau}_t^2$ that minimizes the RMSPE. Repeat step 3 on full data set \mathbf{S}_t by fixing $\phi_t = \hat{\phi}_t$, $\sigma_t^2 = \hat{\sigma}_t^2$. Estimate $\hat{y}_t(\mathbf{S}_t^*)$ by posterior mean

$$\tilde{\hat{y}}_t(\mathbf{S}_t^*) = \mathbf{1}_{t>1}(t) \mathbf{g}_{t-1}^T(\mathbf{S}_t^*) \hat{\gamma}_{t-1} \hat{y}_{t-1}(\mathbf{S}_t^*) + \mathbf{h}_t^T(\mathbf{S}_t^*) \hat{\beta}_t + V_{t,\mathbf{S}_t^*} \mu_{t,\mathbf{S}_t^*}$$

step 7 For a new input location \mathbf{s}_p , predict $y_t(\mathbf{s}_p)$ by posterior:

$$\hat{y}_{t-1}(\mathbf{s})| \cdot \sim N(\zeta_{t-2} \hat{y}_{t-2}(\mathbf{s}) + \mathbf{h}_{t-1}^T(\mathbf{s}) \beta_{t-1} + V_{t-1,\mathbf{s}} \mu_{t-1,\mathbf{s}}, V_{t-1,\mathbf{s}})$$

Find a confidence interval based on the quantiles of the above distributions.

step 8 Repeat steps 1-7 over all T fidelity levels.

If we fix the values of $\phi_t, \tilde{\tau}_t^2$ and $\hat{y}_t(\mathbf{S}_t)$ first, the covariance matrix $\tilde{\boldsymbol{\Sigma}}_t$ can be calculated by ϕ_t and $\tilde{\tau}_t^2$. We assign an independent conjugate prior for the parameters of each level $p(\beta_t, \sigma_t^2, \gamma_t) = p(\beta_t)p(\sigma_t^2)p(\gamma_t)$ such as $\beta_t \sim N(\boldsymbol{\mu}_{\beta_t}, \sigma_t^2 \mathbf{V}_{\beta_t})$, $\sigma_t^2 \sim IG(a_t, b_t)$, and $\gamma_t \sim N(\boldsymbol{\mu}_{\gamma_t}, \sigma_{t+1}^2 \mathbf{V}_{\gamma_t})$. Based on this specifications, the posterior density function can be separated for each level t as:

$$\begin{aligned} p(\beta_t, \gamma_{t-1}, \sigma_t^2 | \mathbf{Z}_t, \hat{y}_{t-1}(\mathbf{S}_t)) &\propto IG(\sigma_t^2 | a_t, b_t) N(\beta_t | \boldsymbol{\mu}_{\beta_t}, \sigma_t^2 \mathbf{V}_{\beta_t}) N(\gamma_{t-1} | \boldsymbol{\mu}_{\gamma_{t-1}}, \sigma_t^2 \mathbf{V}_{\gamma_{t-1}}) \\ &\times N(\mathbf{Z}_t | \zeta_{t-1}(\mathbf{S}_t) \circ \hat{y}_{t-1}(\mathbf{S}_t) + \mathbf{h}_t^T \beta_t, \sigma_t^2 \tilde{\boldsymbol{\Sigma}}_t). \end{aligned} \quad (4.8)$$

We can compute the full conditional density function of γ_{t-1}, β_t , and σ_t^2 as

$$\gamma_{t-1} | \beta_t, \sigma_t^2, \mathbf{Z}_t, \hat{y}_{t-1}(\mathbf{S}_t) \sim N(\gamma_{t-1} | \tilde{\mathbf{V}}_{\gamma_{t-1}} \tilde{\boldsymbol{\mu}}_{\gamma_{t-1}}, \sigma_t^2 \tilde{\mathbf{V}}_{\gamma_{t-1}}), \quad (4.9)$$

$$\beta_t | \sigma_t^2, \mathbf{Z}_t, \hat{y}_{t-1}(\mathbf{S}_t) \sim N(\beta_t | \tilde{\mathbf{V}}_{\beta_t} \tilde{\boldsymbol{\mu}}_{\beta_t}, \sigma_t^2 \tilde{\mathbf{V}}_{\beta_t}) \quad (4.10)$$

$$\sigma_t^2 | \mathbf{Z}_t, \hat{y}_{t-1}(\mathbf{S}_t) \sim IG(\sigma_t^2 | a_t^*, b_t^*) \quad (4.11)$$

were $\tilde{\mathbf{V}}_{\gamma_{t-1}}, \tilde{\boldsymbol{\mu}}_{\gamma_{t-1}}, \tilde{\mathbf{V}}_{\beta_t}, \tilde{\boldsymbol{\mu}}_{\beta_t}, \sigma_t^2 \tilde{\mathbf{V}}_{\beta_t}, a_t^*$, and b_t^* are given analytically in Appendix D. Note that for $t = 1$, γ_0 and $y_0(\mathbf{S}_t)$ do not exist. Also the conditional posterior density function of β_1 and σ_1^2 are slightly different as explained in Appendix D.

A K -fold cross-validation method is used for the selection of optimal values for the parameters ϕ_t and $\tilde{\tau}_t^2$ at level t that provide best prediction performance for the model, from a group of candidates. The criteria of choosing ϕ_t and $\tilde{\tau}_t^2$ can be the root mean square prediction error (RMSPE) over the K folds of data set. The geolocated observations of the t fidelity are partitioned into K equal size subsets. Then, one of the subsets is used as a test set and the others are used for training. The procedure is repeated K times such that each subset is used once as a test set. The computational complexity of these procedures is reduced significantly from the use of the nearest neighbors Gaussian process priors in the recursive co-kriging model. The estimation, tuning and prediction procedure of conjugate RNNC model are given in Algorithm 1. Similar to other NNCGP models, the conjugate RNNC model analyzes the data set of each fidelity level sequentially from the lowest level to the highest. For each single fidelity level t , the conjugate RNNC model is able to run in parallel for tuning the parameter ϕ_t and τ_t^2 and K fold cross validation procedure. Thus, the computational complexity is only $\mathcal{O}(\tilde{n}_1 m^3)$ for each run in a parallel computing environment, which makes the conjugate RNNC model an extremely fast algorithm. Compared to the MCMC based NNCGP models, it is obvious that the conjugate RNNC model provides an empirical estimation of spatial effect parameter ϕ_t and noise parameter $\tilde{\tau}_t^2$ with a crude resolution, meanwhile, the prediction performance of conjugate RNNC model relies on the choice of the candidates of ϕ_t and $\tilde{\tau}_t^2$. For applications that require very precise estimation of covariance parameters, such as emulating some physical science and engineering computer models, the conjugate RNNC model may not be the first choice compared to other RNNC models. However, for large data applications whose main focus is on providing moderate predictions in a limited time and there is less interest in the inference about the covariance, the conjugate RNNC model provides satisfying outputs with extremely fast speed. We note that the proposed MCMC free inference can be viewed as a sequential optimization technique which splits the parametric space into several lower dimension components where we can apply conditional independent conjugate NNCGP models.

5 Synthetic Data Example and Real Data Analysis

We study the performance of our proposed procedures, the conjugate RNNC and the collapsed RNNC, as well as compare their performances with that of the sequential NNCGP. The empirical study is based on a synthetic data set example once with nested and once with non-nested input data sets. and based on a real satellite data set application. As measures of performance we use the root mean squared prediction errors (RMSPE), coverage probability of the 95% equal tail credible interval (CVG(95%)), average length of the 95% equal tail credible interval (ALCI(95%)), and continuous rank probability score (CRPS) (Gneiting and Raftery, 2007). The simulations were performed in MATLAB R2018a, on a personal computer with specifications (intelR i7-3770 3.4GHz Processor, RAM 8.00GB, MS Windows 64bit).

5.1 Simulation Study

We consider a two-fidelity level system represented by the hierarchical statistical model (3.1) defined on a two dimensional unit square domain with univariate observation data sets for both \mathbf{Z}_1 and \mathbf{Z}_2 . Let the design matrix be $\mathbf{h}(\mathbf{S}_t) = \mathbf{1}$, the autoregressive coefficient function be an unknown constant $\zeta_1(s) = \gamma_1$, and exponential covariance

functions. We generate two synthetic data sets for the above statistical model. The true values of the parameters are listed in Table 1 and Table 3. The data sets on the nested spatial locations consists of observations \mathbf{Z}_1 and \mathbf{Z}_2 from 100×100 grids \mathbf{S}_1 and \mathbf{S}_2 , respectively. The data sets, shown in Figures 2a and 2b are based on a fully non-nested input where the low fidelity observations \mathbf{Z}_1 and the high fidelity observations \mathbf{Z}_2 are generated at irregularly located at point in sets \mathbf{S}_1 and \mathbf{S}_2 of size 5000, while $\mathbf{S}_1 \cap \mathbf{S}_2 = \emptyset$. In all data sets, a few small square regions from \mathbf{Z}_2 are treated as a testing data-set, and the rest of \mathbf{Z}_2 and \mathbf{Z}_1 are treated as training data sets. The testing regions for the non-nested input can be seen as white boxes in Figure 2(b).

Regarding the Bayesian inference, we compared the sequential NNCGP model, with the proposed recursive collapsed RNNC model and that with the recursive conjugate RNNC model, on both nested and non-nested data sets. We assigned similar non-informative priors for all the four models. We assign independent conjugate prior on parameters $\beta_1 \sim N(0, 1000)$, $\beta_2 \sim N(0, 1000)$, and scale parameter γ_1 . We assign independent inverse gamma prior on spatial variance parameters $\sigma_1^2 \sim IG(2, 1)$, and $\sigma_2^2 \sim IG(2, 1)$ and on the noise parameters $\tau_1^2 \sim IG(2, 1)$, $\tau_2^2 \sim IG(2, 1)$. We also assign uniform prior on the range parameters $\phi_1 \sim U(0, 100)$, and $\phi_2 \sim U(0, 100)$. For the collapsed RNNC model, we run Markov chain Monte Carlo (MCMC) samplers for 35000 iterations where the first 5000 iterations are discarded as a burn-in, and convergence of the MCMC sampler was diagnosed from the individual trace plots. The RMSPE with a 5-fold cross-validation was used for the conjugate RNNC model, we select ϕ_t from the range $[0.1, 20]$, and $\tilde{\tau}_t^2$ from the range $[0.005, 0.5]$. No significant differences were observed when we used 3-fold cross-validation and 7-fold cross-validation approach.

| | True values | Nested data-set | | | | |
|--------------|-------------|------------------|---------------|----------------|---------------|----------------|
| | | Sequential NNCGP | | Collapsed RNNC | | Conjugate RNNC |
| β_1 | 10 | 10.29 | (9.93,10.57) | 9.96 | (9.60,10.32) | 10.02 |
| β_2 | 1 | 0.77 | (0.59,1.04) | 0.87 | (0.59,1.13) | 0.82 |
| σ_1^2 | 4 | 3.55 | (2.77,4.38) | 3.46 | (2.96,4.27) | 3.15 |
| σ_2^2 | 1 | 0.81 | (0.27, 2.05) | 0.98 | (0.43, 1.88) | 0.79 |
| $1/\phi_1$ | 10 | 10.42 | (8.15,13.47) | 10.50 | (8.59,13.90) | 12.1 |
| $1/\phi_2$ | 10 | 14.96 | (3.37, 20.29) | 15.69 | (5.92, 19.98) | 19.6 |
| γ_1 | 1 | 0.991 | (0.982,1.003) | 0.991 | (0.976,1.004) | 0.992 |
| τ_1^2 | 0.1 | 0.121 | (0.098,0.138) | 0.153 | (0.099,0.195) | 0.125 |
| τ_2^2 | 0.05 | 0.067 | (0.033,0.106) | 0.099 | (0.041,0.194) | 0.158 |
| m | 10 | - | - | - | - | - |

Table 1: The estimation of parameters in nested input dataset, using sequential NNCGP, collapsed RNNC and conjugate RNNC models.

| | Nested data-set | | |
|------------|------------------|----------------|----------------|
| | Sequential NNCGP | Collapsed RNNC | Conjugate RNNC |
| RMSPE | 0.6278 | 0.6875 | 0.7217 |
| NSME | 0.7664 | 0.7547 | 0.7081 |
| CRPS | 0.4453 | 0.4417 | 0.4102 |
| CVG(95%) | 0.9054 | 0.8761 | 0.9284 |
| ALCI(95%) | 1.9284 | 1.9209 | 2.5377 |
| Time(Hour) | 4.5 | 4.7 | 0.08 |

Table 2: Performance measures for the predictive ability of the sequential NNCGP model, collapsed RNNC model and conjugate RNNC model.

| | True values | Non-nested data-set | | |
|--------------|-------------|----------------------|----------------------|----------------|
| | | Sequential NNCGP | Collapsed RNNC | Conjugate RNNC |
| β_1 | 10 | 9.71 (9.36, 10.16) | 9.97 (9.52, 10.41) | 9.71 |
| β_2 | 1 | 0.87 (0.39, 1.36) | 1.23 (0.24, 2.19) | 1.27 |
| σ_1^2 | 4 | 3.51 (2.71, 4.52) | 3.28 (3.02, 3.72) | 3.84 |
| σ_2^2 | 1 | 1.05 (0.18, 2.31) | 1.00 (0.64, 1.49) | 1.19 |
| $1/\phi_1$ | 10 | 10.77 (8.07, 13.91) | 13.23 (9.93, 15.85) | 5 |
| $1/\phi_2$ | 10 | 12.61 (3.93, 24.07) | 16.01 (12.84, 19.92) | 20 |
| γ_1 | 1 | 0.995 (0.983, 1.051) | 0.967 (0.942, 0.994) | 0.959 |
| τ_1^2 | 0.1 | 0.125 (0.097, 0.148) | 0.102 (0.072, 0.152) | 0.11 |
| τ_2^2 | 0.05 | 0.158 (0.041, 0.232) | 0.182 (0.032, 0.292) | 0.01 |
| m | 10 | - | - | - |

Table 3: The estimation of parameters in non-nested input dataset using sequential NNCGP, collapsed RNNC and conjugate RNNC models.

| | Non-nested data-set | | |
|------------|---------------------|----------------|----------------|
| | Sequential NNCGP | Collapsed RNNC | Conjugate RNNC |
| RMSPE | 0.9319 | 0.9241 | 1.0680 |
| NSME | 0.7489 | 0.7827 | 0.7480 |
| CRPS | 0.6109 | 0.6110 | 0.6516 |
| CVG(95%) | 0.9286 | 0.9714 | 0.9538 |
| ALCI(95%) | 1.4855 | 1.7612 | 2.4885 |
| Time(Hour) | 4.1 | 4.3 | 0.05 |

Table 4: Performance measures for the predictive ability of the Sequential NNCGP model, collapsed RNNC model and conjugate RNNC model, in non-nested input.

In Tables 1 and 3, we report the Monte Carlo estimates of the posterior means and the associated 95% marginal credible intervals of the unknown parameters using the two different NNCGP based procedures: sequential NNCGP, collapsed RNNC, along with the posterior mean and tuned values of parameters using conjugate RNNC, with $m = 10$. There is no significant difference in the estimation of parameters for all MCMC based models (NNCGP and collapsed RNNC) and the true values of the parameters are successfully included in the 95% marginal credible intervals. The introduction of latent interpolants may have caused a small overestimation of τ_2^2 for all models. Instead, the conjugate RNNC is underestimating the variance of the nugget for the second fidelity level. This underestimation seems to be associated with the relatively better approximate the CVG but also with the large ALC. The uncertainty in the parameter estimations can be improved with a semi-nested or nested structure between the observed locations of the fidelity levels, and it is also shown for the auto-regressive co-kriging model in Konomi and Karagiannis (2021). Results also showed that when select ϕ_t and τ_t^2 corresponding to minimized RMSPE, the MCMC free conjugate RNNC model has similar estimation of other parameters comparing to NNCGP and RNNC models. We also observe that the conjugate RNNC model prefers larger value of τ_2^2 when minimizing RMSPE, which is consistent with the previous discussion on NNCGP models.

In Table 2 and Table 4, we report standard performance measures (defined in the Appendix) for the sequential NNCGP, collapsed RNNC and conjugate RNNC with $m = 10$ number of neighbours. All performance measures indicate that the collapsed RNNC model has similar predictive ability with the sequential NNCGP model. The conjugate RNNC model produced RMSPE value that is 10% larger than other NNCGP and collapsed RNNC models, but it is still significantly smaller than the RMSPE values from single level NNCGP and combined NNCGP. The tables also shows that the running time of collapsed RNNC model is not different from sequential NNCGP model, this is consistent with our previous

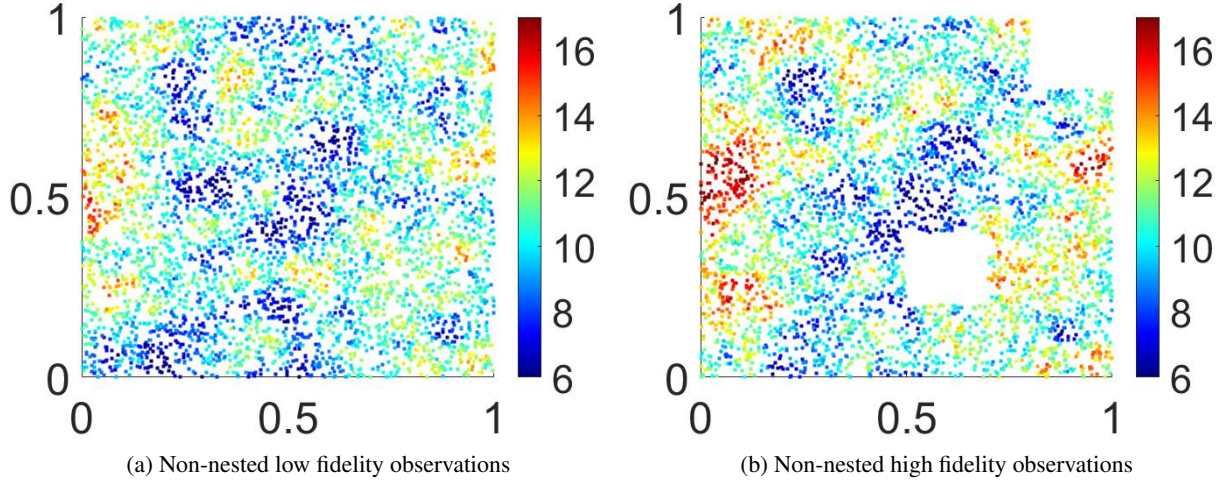


Figure 2: Observations for two fidelity level structure of nested and non-nested observed input space. White boxes indicate the testing regions.

discussion since the two procedures have the same computational complexity. We observe that the conjugate RNNC model has extremely smaller running time compared to sequential NNCGP models, since the inference for conjugate RNNC model requires the same amount of running time as one iteration in collapsed RNNC model. It is worth pointing out that the cross validation process and tuning process in Algorithm 1 are independent from each other, which makes conjugate RNNC model benefit from parallel computation environments and greatly reduce computational time.

Figure 2 and 3 provide the non-nested synthetic observations and the prediction plots from sequential NNCGP, collapsed RNNC, conjugate RNNC, combined NNGP and single level NNGP models. We observed that for the testing regions the NNCGP models provides similar prediction surfaces and all NNCGP models has the better presentation of patterns in prediction surface comparing to single level NNGP model.

5.2 Application to High-resolution Infrared Radiation Sounder data

We model our data based on the two-fidelity level conjugate RNNC model and on the two-fidelity level sequential NNCGP model. Moreover, we provide comparisons with the single level NNGP model and combined NNGP model. We consider a linear model for the mean of the Gaussian processes, in $y_1(\cdot)$ and $\delta_2(\cdot)$, with linear basis function representation $\mathbf{h}(s_t)$ and coefficients $\beta_t = \{\beta_{0,t}, \beta_{1,t}, \beta_{2,t}\}^T$. We consider the scalar discrepancy $\zeta(s)$ to be unknown constant and equal to γ . The number of nearest neighbors m is set to 10, and the spatial process \mathbf{w}_t is consider to have a diagonal anisotropic exponential covariance function.

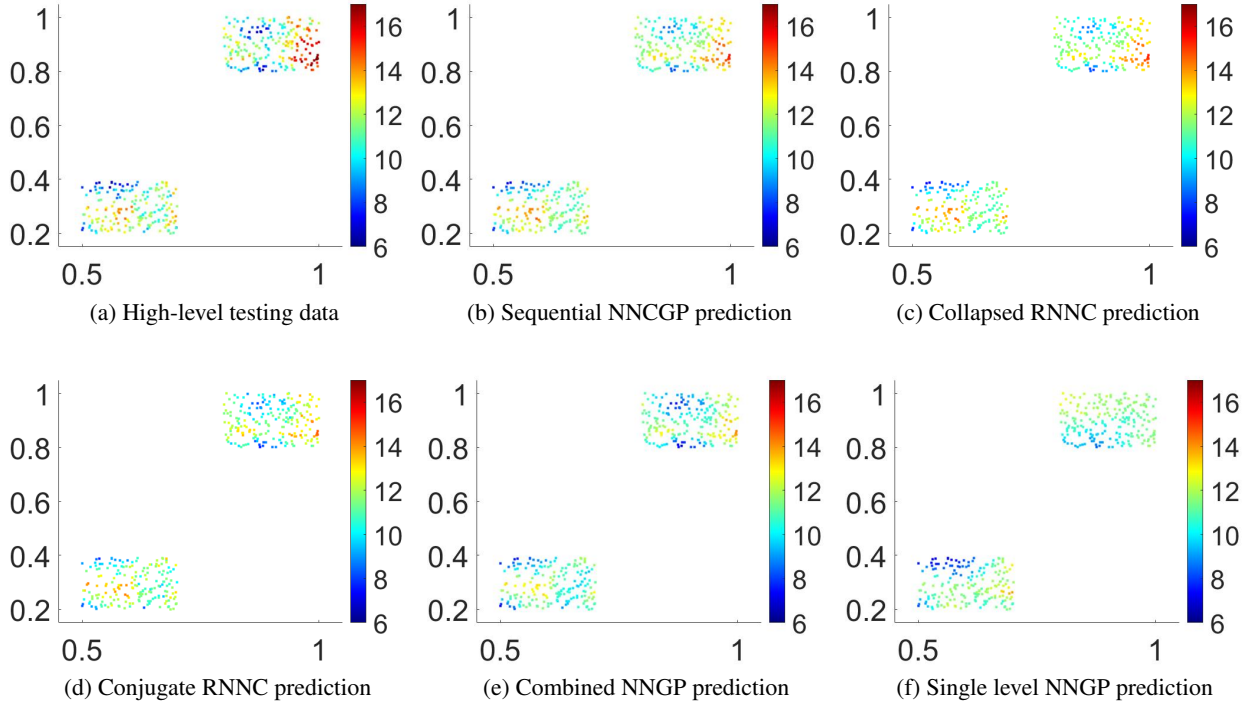


Figure 3: Non-nested input observations with two fidelity level structure. Original testing data (a) along with predictions of the high fidelity level data-set by (b) Sequential NNCGP, (c) Collapsed RNNC, (d) Conjugate RNNC, (e) Combined NNGP and (f) single level NNGP.

| | Model | | | | |
|------------|------------------|-------------------|---------------|----------------|----------------|
| | Sequential NNCGP | Single level NNGP | Combined NNGP | Collapsed RNNC | Conjugate RNNC |
| RMSPE | 1.2044 | 1.8153 | 1.6772 | 1.2113 | 1.3606 |
| NSME | 0.8439 | 0.5499 | 0.6726 | 0.8487 | 0.8198 |
| CRPS | 0.7023 | 1.6498 | 0.9274 | 0.6767 | 0.7475 |
| CVG(95%) | 0.9255 | 0.8350 | 0.9197 | 0.9398 | 0.9443 |
| ALCI(95%) | 3.094 | 4.214 | 5.778 | 3.162 | 4.392 |
| Time(Hour) | 38 | 20 | 32 | 40 | 0.3 |

Table 5: Performance measures for the predictive ability of sequential NNCGP, single level NNGP, combined NNGP, collapsed RNNC and conjugate RNNC models in NOAA 14 and NOAA 15 HIRS instrument data analysis.

We assign independent normal distribution priors with zero mean and large variances for $\beta_{0,t}, \beta_{1,t}, \beta_{2,t}$ and γ . We assign independent uniform prior distributions $U(0, 1000)$ to the range correlation parameters $(\phi_{t,1}, \phi_{t,2})$ for $t = 1, 2$. Also, we assign independent $IG(2, 1)$ prior distributions for the variance parameters σ_t^2 and τ_t^2 . For the Bayesian inference of the sequential NNCGP, we run the MCMC sampler with of 35,000 iterations where the first 5,000 iterations are discarded as a burn-in. For the Bayesian inference of conjugate RNNC, we consider using posterior means as the estimated values for parameters $\beta_{0,t}, \beta_{1,t}, \beta_{2,t}, \sigma_t^2$ and γ ; we also use posterior means as the imputation values for latent process $\tilde{\mathbf{y}}_t$ and for the prediction values of $z(s_p)$ at location $s_p \notin \tilde{\mathbf{S}}_t$.

The prediction performance metrics of the four different methods are given in Table 5. Compared to the single level NNGP model and combined NNGP model, the sequential NNCGP model and conjugate RNNC model produced a

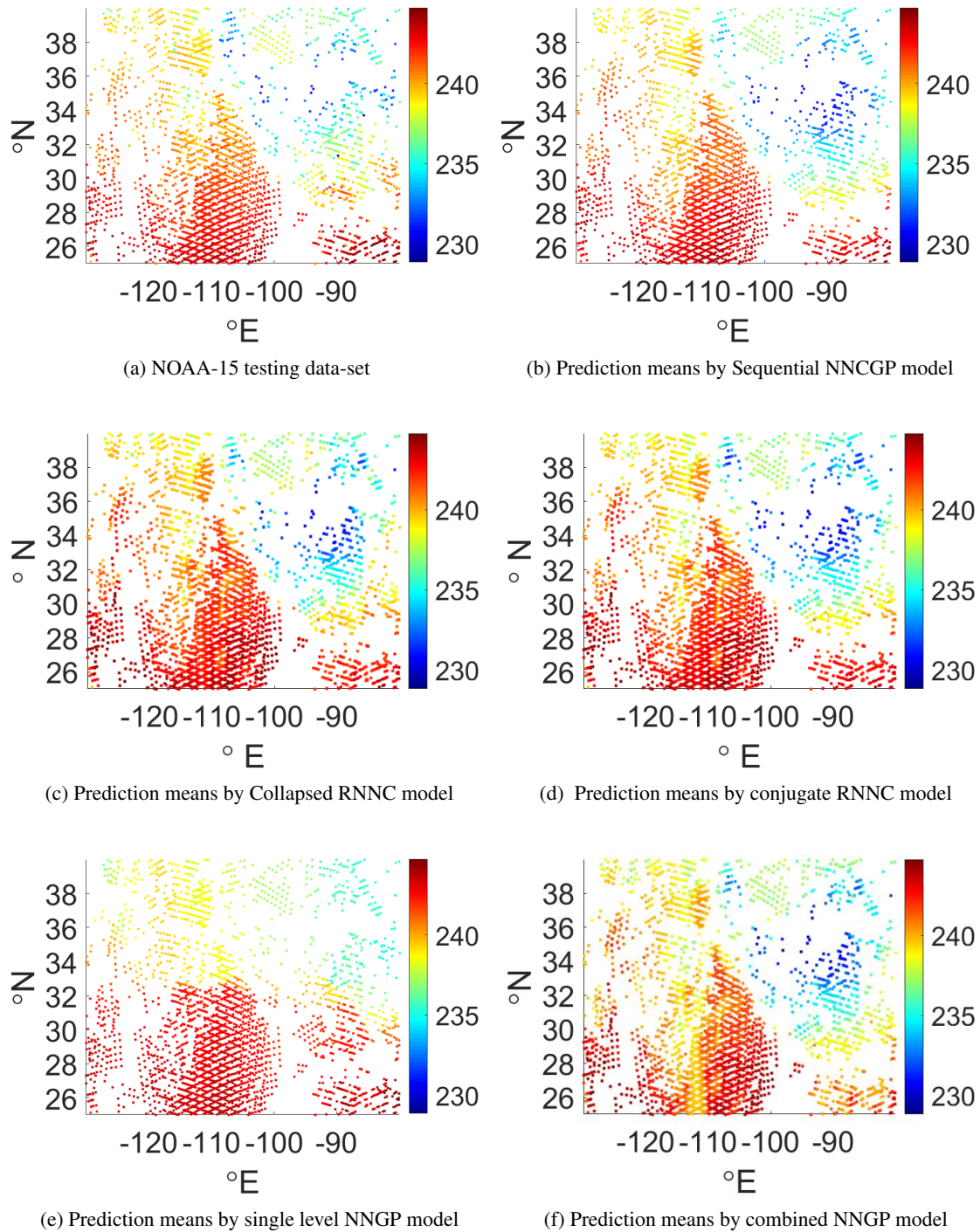


Figure 4: Predictions of NOAA-15 Brightness Temperatures(K) testing data-set by (b) sequential NNCGP, (c) collapsed RNNC, (d) conjugate RNNC, (e) single level NNGP and (f) combined NNGP models.

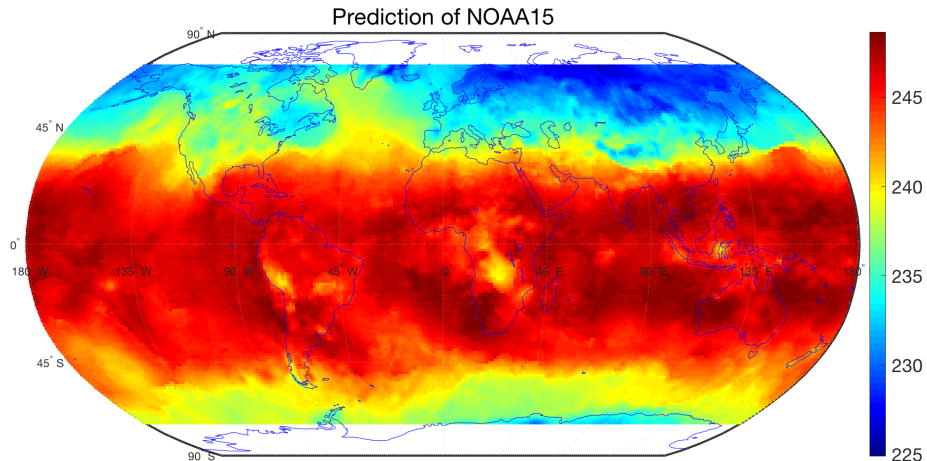


Figure 5: The global prediction brightness temperature values of NOAA 15 using the MCMC free conjugate model.

20-30% smaller RMSPE and their NSME is closer to 1. The sequential NNCGP model and collapsed RNNC model also produced larger CVG and smaller ALCI than the single level NNGP model and combined NNGP model. The result suggests that the NNCGP and RNNC models have a substantial improvement in terms of predictive accuracy in real data analysis too. In the prediction plots (Figure 4) of the testing data of NOAA-15, we observe that RNNC models are more capable of capturing the pattern of the testing data than single level NNGP model and combined NNGP model. This is reasonable because the observations from NOAA-14 have provided information of the testing region, and comparing to combined NNGP model, the NNCGP and RNNC models are capable of modeling the discrepancy of observations from different satellites. In the non-nested structure, the computational complexity of the single level NNGP model is $\mathcal{O}(n_2 m^3)$ and that of NNCGP model is $\mathcal{O}((n_1 + n_2) m^3)$, for an MCMC iteration. However, the whole computational complexity of the conjugate RNNC model is $\mathcal{O}((n_1 + n_2) m^3)$ with parallel computational environment, which makes it remarkably computationally efficient without losing significant prediction accuracy. This is consistent with the running times of the models shown in Table 5.

We apply the MCMC free conjugate RNNC model for gap-filling predictions based upon a discrete global grid. We chose to use 1° latitude by 1.25° longitude ($1^\circ \times 1.25^\circ$) pixels as grids with global spatial coverage from -70° to 70° N. By applying the NNCGP model, we predict gridded NOAA-15 brightness temperature data on the center of the grids, based on the NOAA-14 and NOAA-15 swath-based spatial support. The prediction plot (Figure 5) illustrates the ability of the MCMC free conjugate RNNC model to handle large irregularly spaced data sets and produce a gap-filled composite gridded dataset. The resulting global image of the brightness temperature is practically the same as the sequential NNCGP.

6 Summary and conclusions

We have proposed a new computationally efficient co-kriging method, the recursive nearest neighbor Autoregressive Co-Kriging (RNNC) model, for the analysis of large and multi-fidelity spatial data sets. In particular, we proposed two computationally efficient inferential versions of it the collapsed RNNC and the conjugate RNNC. For the collapsed RNNC, we integrate out the latent variables of the RNNC model which enables the factorisation of the likelihood into terms involving smaller and sparse covariance matrices within each level. Then, a prediction focused approximation is applied on the aforesaid model to further speed up the computation. The idea is that cross-validation using grid search on a two or three dimensional space is a computationally feasible method to estimate the hyperparameters. The proposed conjugate RNNC is MCMC free and at most computationally linear in the total number of all spatial locations of all fidelity levels. Both of the proposed procedures, have similarities to modularization approach in Bayesian statistics Bayarri et al. (2009) where the analysis is done in steps rather than jointly. We compared the proposed collapsed RNNC and conjugate RNNC with NNCGP in a simulation study and a real data application of intersatellite calibration. We observed that similar to NNCGP, the collapsed and conjugate RNNC were also able to improve the accuracy of the prediction for the HIRS brightness temperatures from the NOAA-15 polar-orbiting satellite by incorporating information from an older version of the same HIRS sensor on board the polar orbiting satellite NOAA-14.

The proposed procedures can be used for a variety of large multi-fidelity data sets in remote sensing with overlapping areas of observed locations. One can use more complex Vecchias approximations (Vecchia, 1988; Stein et al., 2004; Guinness, 2018; Katzfuss et al., 2020), similar to the NNGP priors, where the ordering of the data can be more complicated but can result in a better approximation. These Vecchias approximation techniques of ordering can be applied naturally in the proposed RNNC model, however, they are out of the scope of this paper and can be investigated in a future work. As a future research, the proposed method can be also extended in the multivariate setting by using ideas from parallel partial autoregressive co-kriging (Ma et al., 2022) and NNGP spatial factor models (Taylor-Rodriguez et al., 2018). One way to introduce non-stationarity is by using treed based model such as in Konomi et al. (2014). Still, work needs to be done in developing new strategies for tuning the hyperparameters in more complex covariance functions with multiple parameters within a fidelity level.

Acknowledgements

The research of Konomi and Kang was partially supported by National Science Foundation grant NSF DMS-2053668. Kang was also partially supported by Simons Foundation’s Collaboration Award (#317298 and #712755), and the Taft Research Center at the University of Cincinnati.

References

- Bayarri, M. J., Berger, J. O., and Liu, F. (2009), “Modularization in Bayesian analysis, with emphasis on analysis of computer models,” *Bayesian Analysis*, 4, 119 – 150, URL <https://doi.org/10.1214/09-BA404>.
- Chander, G., Hewison, T., Fox, N., Wu, X., Xiong, X., and Blackwell, W. (2013), “Overview of Intercalibration of Satellite Instruments,” *IEEE Transactions on Geoscience and Remote Sensing*, 51:3, 1056–1080.

- Cheng, S., Konomi, B. A., Matthews, J. L., Karagiannis, G., and Kang, E. L. (2021), “Hierarchical Bayesian nearest neighbor co-kriging Gaussian process models; an application to intersatellite calibration,” *Spatial Statistics*, 44, 100516, URL <https://www.sciencedirect.com/science/article/pii/S2211675321000269>.
- Cressie, N. and Johannesson, G. (2008), “Fixed rank kriging for very large spatial data sets,” *Journal of the Royal Statistical Society: Series B (Statistical Methodology)*, 70, 209–226.
- Datta, A., Banerjee, S., Finley, A. O., and Gelfand, A. E. (2016), “Hierarchical nearest-neighbor Gaussian process models for large geostatistical datasets,” *Journal of the American Statistical Association*, 111, 800–812.
- Finley, A. O., Datta, A., Cook, B. D., Morton, D. C., Andersen, H. E., and Banerjee, S. (2019a), “Efficient Algorithms for Bayesian Nearest Neighbor Gaussian Processes,” *Journal of Computational and Graphical Statistics*, 28, 401–414, URL <https://doi.org/10.1080/10618600.2018.1537924>. PMID: 31543693.
- (2019b), “Efficient algorithms for Bayesian nearest neighbor Gaussian processes,” *Journal of Computational and Graphical Statistics*, 1–14.
- Gneiting, T. and Raftery, A. E. (2007), “Strictly Proper Scoring Rules, Prediction, and Estimation,” *Journal of the American Statistical Association*, 102, 359–378.
- Goldberg, M., e. a. (2011), “The Global Space-Based Inter-Calibration Systems,” *Bull. Am. Meteorol. Soc.*, 92, 467–475.
- Guinness, J. (2018), “Permutation and Grouping Methods for Sharpening Gaussian Process Approximations,” *Technometrics*, 60, 415–429, URL <https://doi.org/10.1080/00401706.2018.1437476>. PMID: 31447491.
- Jackson, D., Wylie, D., and Bates, J. (2003), “The HIRS pathfinder radiance data set (1979–2001),” in *Proc. of the 12th Conference on Satellite Meteorology and Oceanography, Long Beach, CA, USA, 10-13 February 2003*, volume 5805 of *LNCSS*, Springer.
- Katzfuss, M., Guinness, J., Gong, W., and Zilber, D. (2020), “Vecchia Approximations of Gaussian-Process Predictions,” *Journal of Agricultural, Biological and Environmental Statistics*, 25, 383–414.
- Kennedy, M. C. and O’Hagan, A. (2000), “Predicting the output from a complex computer code when fast approximations are available,” *Biometrika*, 87, 1–13.
- Konomi, B. A., Kang, E. L., Almomani, A., and Hobbs, J. (2023), “Bayesian Latent Variable Co-kriging Model in Remote Sensing for Quality Flagged Observations,” *Journal of Agricultural, Biological and Environmental Statistics*, 4, 119 – 150, URL <https://doi.org/10.1007/s13253-023-00530-9>.
- Konomi, B. A. and Karagiannis, G. (2021), “Bayesian Analysis of Multifidelity Computer Models With Local Features and Nonnested Experimental Designs: Application to the WRF Model,” *Technometrics*, 63, 510–522, URL <https://doi.org/10.1080/00401706.2020.1855253>.
- Konomi, B. A., Sang, H., and Mallick, B. K. (2014), “Adaptive Bayesian Nonstationary Modeling for Large Spatial Datasets Using Covariance Approximations,” *Journal of Computational and Graphical Statistics*, 23, 802–829.
- Le Gratiet, L. (2013), “Bayesian analysis of hierarchical multifidelity codes,” *SIAM/ASA Journal on Uncertainty Quantification*, 1, 244–269.
- Le Gratiet, L. and Garnier, J. (2014), “Recursive co-kriging model for design of computer experiments with multiple levels of fidelity,” *International Journal for Uncertainty Quantification*, 4.
- Liu, J. S., Wong, W. H., and Kong, A. (1994), “Covariance structure of the Gibbs sampler with applications to the comparisons of estimators and augmentation schemes,” *Biometrika*, 81, 27–40, URL <https://doi.org/10.1093/biomet/81.1.27>.
- Ma, P., Karagiannis, G., Konomi, B. A., Asher, T. G., Toro, G. R., and Cox, A. T. (2022), “Multifidelity computer model emulation with high-dimensional output: An application to storm surge,” *Journal of the Royal Statistical Society: Series C (Applied Statistics)*, n/a, URL <https://rss.onlinelibrary.wiley.com/doi/abs/10.1111/rssc.12558>.
- National Research Council (2004), *Climate Data Records from Environmental Satellites: Interim Report*, Washington, DC: The National Academies Press, URL <https://www.nap.edu/catalog/10944/climate-data-records-from-environmental-satellites-interim-report>.
- Nguyen, H., Cressie, N., and Braverman, A. (2012), “Spatial statistical data fusion for remote sensing applications,” *Journal of the American Statistical Association*, 107, 1004–1018.
- (2017), “Multivariate spatial data fusion for very large remote sensing datasets,” *Remote Sensing*, 9, 142.

- O'Hagan, A. (1998), "A Markov property for covariance structures," *Statistics Research Report*, 98, 510.
- Qian, Z., Seepersad, C. C., Joseph, V. R., Allen, J. K., and Jeff Wu, C. F. (2005), "Building Surrogate Models Based on Detailed and Approximate Simulations," *Journal of Mechanical Design*, 128, 668–677, URL <https://doi.org/10.1115/1.2179459>.
- Stein, M. L. (2014), "Limitations on low rank approximations for covariance matrices of spatial data," *Spatial Statistics*, 8, 1–19.
- Stein, M. L., Chi, Z., and Welty, L. J. (2004), "Approximating likelihoods for large spatial data sets," *Journal of the Royal Statistical Society: Series B (Statistical Methodology)*, 66, 275–296.
- Taylor-Rodriguez, D., Finley, A. O., Datta, A., Babcock, C., Andersen, H.-E., Cook, B. D., Morton, D. C., and Banerjee, S. (2018), "Spatial Factor Models for High-Dimensional and Large Spatial Data: An Application in Forest Variable Mapping," *arXiv preprint arXiv:1801.02078*.
- Vecchia, A. V. (1988), "Estimation and model identification for continuous spatial processes," *Journal of the Royal Statistical Society: Series B (Methodological)*, 50, 297–312.
- Xiong, X., Cao, C., and Chander, G. (2010), "An overview of sensor calibration inter-comparison and applications," *Frontiers of Earth Science in China*, 4, 237–252.

Appendix

A NNGP specifications

The posterior distribution of

$$\begin{aligned} \tilde{p}(\mathbf{w}_t|\cdot) &\propto \exp \left[-\frac{1}{2} \sum_{i=1}^{n_t} \{w_t(s_{t,i}) - \mathbf{B}_{t,s_{t,i}} \mathbf{w}_{t,N_t(s_{t,i})}\}^T F_{t,s_{t,i}}^{-1} \{w_t(s_{t,i}) - \mathbf{B}_{t,s_{t,i}} \mathbf{w}_{t,N_t(s_{t,i})}\} \right] \\ &= \exp \left(-\frac{1}{2} \mathbf{w}_t^T \mathbf{B}_t^T \mathbf{F}_t^{-1} \mathbf{B}_t \mathbf{w}_t \right), \end{aligned} \quad (\text{A.1})$$

where $\mathbf{F}_t = \text{diag}(F_{t,s_{t,1}}, F_{t,s_{t,2}}, \dots, F_{t,s_{t,n_t}})$, $\mathbf{B}_t = (\mathbf{B}_{t,1}^T, \mathbf{B}_{t,2}^T, \dots, \mathbf{B}_{t,n_t}^T)^T$, and for each element in \mathbf{B}_t , we have $\mathbf{B}_{t,i} = (\mathbf{B}_{t,s_{t,i},1}^T, \mathbf{B}_{t,s_{t,i},2}^T, \dots, \mathbf{B}_{t,s_{t,i},n_t}^T)^T$ and

$$\mathbf{B}_{t,s_{t,i},j} = \begin{cases} 1, & \text{if } i = j, \\ -\mathbf{B}_{t,s_{t,i},k}, & \text{if } s_{t,j} \text{ is the } k^{\text{th}} \text{ element in } N_t(s_{t,i}), \\ 0, & \text{Others.} \end{cases} \quad (\text{A.2})$$

B Mean and Variance Specifications

The mean vector $\boldsymbol{\mu} = (\mu_1(s_{1,1}), \dots, \mu_1(s_{1,n_1}), \dots, \mu_T(s_{T,n_T}))$ is

$$\begin{aligned} \mu_t(s_{t,k}) &= \mathbf{1}_{\{t>1\}}(t) \sum_{i=1}^{t-1} \left\{ \prod_{j=i}^{t-1} \zeta_j(s_{t,k}) \right\} \{ \mathbf{h}_i^T(s_{t,k}) \boldsymbol{\beta}_i + \mathbf{1}_{\{s_{t,k} \in \mathbf{S}_i\}}(s_{t,k}) w_i(s_{t,k}) \} \\ &\quad + \mathbf{h}_t^T(s_{t,k}) \boldsymbol{\beta}_t + w_t(s_{t,k}), \end{aligned} \quad (\text{B.1})$$

for $t = 1, \dots, T$, $i = 1, \dots, n_t$. $\mathbf{1}_{\{\cdot\}}(\cdot)$ is the indicator function, and covariance matrix $\boldsymbol{\Lambda}$ is a block matrix with blocks $\boldsymbol{\Lambda}^{(1,1)}, \dots, \boldsymbol{\Lambda}^{(1,T)}, \dots, \boldsymbol{\Lambda}^{(T,T)}$, and the size of $\boldsymbol{\Lambda}$ is $\sum_{t=1}^T n_t \times \sum_{t=1}^T n_t$. The $\boldsymbol{\Lambda}^{(t,t)}$ components are calculated as:

$$\begin{aligned} \boldsymbol{\Lambda}_{k,l}^{(t,t)} &= \text{cov}(z_t(s_{t,k}), z_t(s_{t,l})|\cdot) = \sum_{i=1}^{t-1} \mathbf{1}_{\{s_{t,k}, s_{t,l} \notin \mathbf{S}_i\}}(s_{t,k}, s_{t,l}) \left\{ \prod_{j=i}^{t-1} \zeta_j(s_{t,k})^T \zeta_j(s_{t,l}) \right\} C_i(s_{t,k}, s_{t,l}|\boldsymbol{\theta}_i) \\ &\quad + \mathbf{1}_{s_{t,k}=s_{t,l}}(s_{t,k}, s_{t,l}) \tau_t^2, \end{aligned}$$

for t and $t' = 1, \dots, T$; $k = 1, \dots, n_t$; $l = 1, \dots, n_{t'}$, and

$$\begin{aligned} \boldsymbol{\Lambda}_{k,l}^{(t,t')} &= \text{cov}(z_t(s_{t,k}), z_{t'}(s_{t',l})|\cdot) = \sum_{i=1}^{\min(t,t')-1} \mathbf{1}_{\{s_{t,k}, s_{t',l} \notin \mathbf{S}_i\}}(s_{t,k}, s_{t',l}) \left\{ \prod_{j=i}^{\min(t,t')-1} \zeta_j(s_{t,k})^T \zeta_j(s_{t',l}) \right\} \\ &\quad \times C_i(s_{t,k}, s_{t',l}|\boldsymbol{\theta}_i) + \mathbf{1}_{\{s_{t,k}, s_{t',l} \notin \mathbf{S}_{\min(t,t')}\}}(s_{t,k}, s_{t',l}) C_{\min(t,t')}(s_{t,k}, s_{t',l}|\boldsymbol{\theta}_{\min(t,t')}), \end{aligned} \quad (\text{B.2})$$

for $t \neq t'$, $\boldsymbol{\Lambda}^{(t,t')}$.

C Gibbs Sampler

$$\begin{aligned} \mathbf{V}_{\beta_t}^* &= (\mathbf{h}_t(\mathbf{S}_t) \tilde{\boldsymbol{\Lambda}}_t(\mathbf{S}_t, \boldsymbol{\theta}_t)^{-1} \mathbf{h}_t^T(\mathbf{S}_t) + \mathbf{V}_{\beta_t}^{-1})^{-1}, \\ \boldsymbol{\mu}_{\beta_t}^* &= \mathbf{V}_{\beta_t}^{-1} \boldsymbol{\mu}_{\beta_t} + \mathbf{h}_t(\mathbf{S}_t) \tilde{\boldsymbol{\Lambda}}_t(\mathbf{S}_t, \boldsymbol{\theta}_t)^{-1} (z_t(\mathbf{S}_t) - \zeta_{t-1}(\mathbf{S}_t) \hat{y}_{t-1}(\mathbf{S}_t)). \end{aligned} \quad (\text{C.1})$$

$$\begin{aligned} \mathbf{V}_{\gamma_t}^* &= \left[(\mathbf{g}_t^T(\mathbf{S}_{t+1}) \hat{y}_t(\mathbf{S}_{t+1}))^T \tilde{\boldsymbol{\Lambda}}_{t+1}(\mathbf{S}_{t+1}, \boldsymbol{\theta}_{t+1}, \tau_{t+1})^{-1} (\mathbf{g}_t^T(\mathbf{S}_{t+1}) \hat{y}_t(\mathbf{S}_{t+1})) + \mathbf{V}_{\gamma_t}^{-1} \right]^{-1}, \\ \boldsymbol{\mu}_{\gamma_t}^* &= \mathbf{V}_{\gamma_t}^{-1} \boldsymbol{\mu}_{\gamma_t} + (\mathbf{g}_t^T(\mathbf{S}_{t+1}) \hat{y}_t(\mathbf{S}_{t+1}))^T \tilde{\boldsymbol{\Lambda}}_{t+1}(\mathbf{S}_{t+1}, \boldsymbol{\theta}_{t+1}, \tau_{t+1})^{-1} (\mathbf{Z}_{t+1} - \mathbf{h}_t^T(\mathbf{S}_{t+1}) \boldsymbol{\beta}_{t+1}). \end{aligned} \quad (\text{C.2})$$

D Gibbs Sampler Conjugate

we derive the posterior distribution as

$$\begin{aligned}
p(\boldsymbol{\beta}_t, \boldsymbol{\gamma}_{t-1}, \sigma_t^2 | \mathbf{Z}_t, \hat{y}_{t-1}(\mathbf{S}_t)) &\propto IG(\sigma_t^2 | a_t, b_t) N(\boldsymbol{\beta}_t | \boldsymbol{\mu}_{\beta_t}, \sigma_t^2 \mathbf{V}_{\beta_t}) N(\boldsymbol{\gamma}_{t-1} | \boldsymbol{\mu}_{\gamma_{t-1}}, \sigma_t^2 \mathbf{V}_{\gamma_{t-1}}) \\
&\quad \times N(\mathbf{Z}_t | \zeta_{t-1}(\mathbf{S}_t) \circ \hat{y}_{t-1}(\mathbf{S}_t) + \mathbf{h}_t^T \boldsymbol{\beta}_t, \sigma_t^2 \tilde{\boldsymbol{\Sigma}}_t) \\
&\propto p(\sigma_t^2 | \mathbf{Z}_t, \hat{y}_{t-1}(\mathbf{S}_t)) p(\boldsymbol{\beta}_t | \sigma_t^2, \mathbf{Z}_t, \hat{y}_{t-1}(\mathbf{S}_t)) p(\boldsymbol{\gamma}_{t-1} | \boldsymbol{\beta}_t, \sigma_t^2, \mathbf{Z}_t, \hat{y}_{t-1}(\mathbf{S}_t)) \\
&\propto (\sigma_t^2)^{a_t+0.5n_t} \exp\left(-\frac{1}{2\sigma_t^2} (\boldsymbol{\beta}_t - \boldsymbol{\mu}_{\beta_t})^T \mathbf{V}_{\beta_t}^{-1} (\boldsymbol{\beta}_t - \boldsymbol{\mu}_{\beta_t})\right) \\
&\quad \times \exp\left(-\frac{1}{2\sigma_t^2} (\boldsymbol{\gamma}_{t-1} - \boldsymbol{\mu}_{\gamma_{t-1}})^T \mathbf{V}_{\gamma_{t-1}}^{-1} (\boldsymbol{\gamma}_{t-1} - \boldsymbol{\mu}_{\gamma_{t-1}})\right) \\
&\quad \times \exp\left(-\frac{1}{2\sigma_t^2} (\mathbf{Z}_t - \mathbf{g}^T(\mathbf{S}_t) \boldsymbol{\gamma}_{t-1} \hat{y}_{t-1}(\mathbf{S}_t) - \mathbf{h}_t^T(\mathbf{S}_t) \boldsymbol{\beta}_t)^T \tilde{\boldsymbol{\Sigma}}_t^{-1} (\mathbf{Z}_t - \mathbf{g}^T(\mathbf{S}_t) \boldsymbol{\gamma}_{t-1} \hat{y}_{t-1}(\mathbf{S}_t) - \mathbf{h}_t^T(\mathbf{S}_t) \boldsymbol{\beta}_t)\right).
\end{aligned}$$

The full conditional density function of $\boldsymbol{\gamma}_{t-1}$ is

$$\begin{aligned}
p(\boldsymbol{\gamma}_{t-1} | \boldsymbol{\beta}_t, \sigma_t^2, \mathbf{Z}_t, \hat{y}_{t-1}(\mathbf{S}_t)) &\propto \exp\left(-\frac{1}{2\sigma_t^2} [\mathbf{g}(\mathbf{S}_t) \boldsymbol{\gamma}_{t-1}^T \hat{y}_{t-1}(\mathbf{S}_t)^T \tilde{\boldsymbol{\Sigma}}_t^{-1} \mathbf{g}^T(\mathbf{S}_t) \boldsymbol{\gamma}_{t-1} \hat{y}_{t-1}(\mathbf{S}_t) \right. \\
&\quad \left. - 2(\mathbf{Z}_t - \mathbf{h}_t^T(\mathbf{S}_t) \boldsymbol{\beta}_t)^T \tilde{\boldsymbol{\Sigma}}_t^{-1} \mathbf{g}^T(\mathbf{S}_t) \boldsymbol{\gamma}_{t-1} \hat{y}_{t-1}(\mathbf{S}_t)]\right) \\
&\propto N(\boldsymbol{\gamma}_{t-1} | \tilde{\mathbf{V}}_{\boldsymbol{\gamma}_{t-1}} \tilde{\boldsymbol{\mu}}_{\boldsymbol{\gamma}_{t-1}}, \sigma^2 \tilde{\mathbf{V}}_{\boldsymbol{\gamma}_{t-1}}), \\
\tilde{\boldsymbol{\mu}}_{\boldsymbol{\gamma}_{t-1}} &= \mathbf{V}_{\boldsymbol{\gamma}_{t-1}}^{-1} \boldsymbol{\mu}_{\boldsymbol{\gamma}_{t-1}} + \mathbf{g}(\mathbf{S}_t) \hat{y}_{t-1}(\mathbf{S}_t)^T \tilde{\boldsymbol{\Sigma}}_t^{-1} (\mathbf{Z}_t - \mathbf{h}_t^T(\mathbf{S}_t) \boldsymbol{\beta}_t), \\
\tilde{\mathbf{V}}_{\boldsymbol{\gamma}_{t-1}} &= \left(\mathbf{V}_{\boldsymbol{\gamma}_{t-1}}^{-1} + \mathbf{g}(\mathbf{S}_t) \hat{y}_{t-1}(\mathbf{S}_t)^T \tilde{\boldsymbol{\Sigma}}_t^{-1} \hat{y}_{t-1}(\mathbf{S}_t) \mathbf{g}^T(\mathbf{S}_t)\right)^{-1}. \tag{D.1}
\end{aligned}$$

After integrate $\boldsymbol{\gamma}_{t-1}$ out, the conditional posterior density function of $\boldsymbol{\beta}_t$ is

$$\begin{aligned}
p(\boldsymbol{\beta}_t | \sigma_t^2, \mathbf{Z}_t, \hat{y}_{t-1}(\mathbf{S}_t)) &\propto \exp\left(-\frac{1}{2\sigma_t^2} [(\mathbf{h}_t^T(\mathbf{S}_t) \boldsymbol{\beta}_t)^T \tilde{\boldsymbol{\Sigma}}_t^{-1} (\mathbf{h}_t^T(\mathbf{S}_t) \boldsymbol{\beta}_t) - 2\mathbf{Z}_t^T \tilde{\boldsymbol{\Sigma}}_t^{-1} \mathbf{h}_t^T(\mathbf{S}_t) \boldsymbol{\beta}_t]\right) \\
&\quad \times \exp\left(-\frac{1}{2\sigma_t^2} (\boldsymbol{\beta}_t - \boldsymbol{\mu}_{\beta_t})^T \mathbf{V}_{\beta_t}^{-1} (\boldsymbol{\beta}_t - \boldsymbol{\mu}_{\beta_t})\right) \exp\left(\frac{1}{2\sigma_t^2} \tilde{\boldsymbol{\mu}}_{\boldsymbol{\gamma}_{t-1}}^T \tilde{\mathbf{V}}_{\boldsymbol{\gamma}_{t-1}} \tilde{\boldsymbol{\mu}}_{\boldsymbol{\gamma}_{t-1}}\right), \\
&\propto N(\boldsymbol{\beta}_t | \tilde{\mathbf{V}}_{\boldsymbol{\beta}_t} \tilde{\boldsymbol{\mu}}_{\boldsymbol{\beta}_t}, \sigma_t^2 \tilde{\mathbf{V}}_{\boldsymbol{\beta}_t}), \\
\tilde{\boldsymbol{\mu}}_{\boldsymbol{\beta}_t} &= \mathbf{V}_{\boldsymbol{\beta}_t}^{-1} \boldsymbol{\mu}_{\boldsymbol{\beta}_t} + \mathbf{h}_t(\mathbf{S}_t) \tilde{\boldsymbol{\Sigma}}_t^{-1} \mathbf{Z}_t - (\mathbf{g}(\mathbf{S}_t) \hat{y}_{t-1}(\mathbf{S}_t)^T \tilde{\boldsymbol{\Sigma}}_t^{-1} \mathbf{h}_t^T(\mathbf{S}_t))^T \tilde{\mathbf{V}}_{\boldsymbol{\gamma}_{t-1}} (\mathbf{V}_{\boldsymbol{\gamma}_{t-1}}^{-1} \boldsymbol{\mu}_{\boldsymbol{\gamma}_{t-1}} \\
&\quad + \mathbf{g}(\mathbf{S}_t) \hat{y}_{t-1}(\mathbf{S}_t)^T \tilde{\boldsymbol{\Sigma}}_t^{-1} \mathbf{Z}_t), \\
\tilde{\mathbf{V}}_{\boldsymbol{\beta}_t} &= \left(\mathbf{V}_{\boldsymbol{\beta}_t}^{-1} + \mathbf{h}(\mathbf{S}_t) \tilde{\boldsymbol{\Sigma}}_t^{-1} \mathbf{h}(\mathbf{S}_t)^T - (\mathbf{g}(\mathbf{S}_t) \hat{y}_{t-1}(\mathbf{S}_t)^T \tilde{\boldsymbol{\Sigma}}_t^{-1} \mathbf{h}_t^T(\mathbf{S}_t))^T \tilde{\mathbf{V}}_{\boldsymbol{\gamma}_{t-1}} (\mathbf{g}(\mathbf{S}_t) \hat{y}_{t-1}(\mathbf{S}_t)^T \tilde{\boldsymbol{\Sigma}}_t^{-1} \mathbf{h}_t^T(\mathbf{S}_t))\right)^{-1}. \tag{D.2}
\end{aligned}$$

The marginalized posterior density function of σ_t is

$$\begin{aligned}
p(\sigma_t^2 | \mathbf{Z}_t, \hat{y}_{t-1}(\mathbf{S}_t)) &\propto \sigma_t^{-a_t-0.5n_t} \exp\left(-\frac{1}{2\sigma_t^2} \left[2b_t + \mathbf{Z}_t^T \tilde{\boldsymbol{\Sigma}}_t^{-1} \mathbf{Z}_t + \boldsymbol{\mu}_{\beta_t}^T \mathbf{V}_{\beta_t}^{-1} \boldsymbol{\mu}_{\beta_t} + \boldsymbol{\mu}_{\boldsymbol{\gamma}_{t-1}}^T \mathbf{V}_{\boldsymbol{\gamma}_{t-1}}^{-1} \boldsymbol{\mu}_{\boldsymbol{\gamma}_{t-1}} - \tilde{\boldsymbol{\mu}}_{\boldsymbol{\beta}_t}^T \tilde{\mathbf{V}}_{\boldsymbol{\beta}_t} \tilde{\boldsymbol{\mu}}_{\boldsymbol{\beta}_t} \right. \right. \\
&\quad \left. \left. - (\mathbf{V}_{\boldsymbol{\gamma}_{t-1}}^{-1} \boldsymbol{\mu}_{\boldsymbol{\gamma}_{t-1}} + \mathbf{g}(\mathbf{S}_t) \hat{y}_{t-1}(\mathbf{S}_t)^T \tilde{\boldsymbol{\Sigma}}_t^{-1} \mathbf{Z}_t)^T \tilde{\mathbf{V}}_{\boldsymbol{\gamma}_{t-1}} (\mathbf{V}_{\boldsymbol{\gamma}_{t-1}}^{-1} \boldsymbol{\mu}_{\boldsymbol{\gamma}_{t-1}} + \mathbf{g}(\mathbf{S}_t) \hat{y}_{t-1}(\mathbf{S}_t)^T \tilde{\boldsymbol{\Sigma}}_t^{-1} \mathbf{Z}_t)\right]\right), \\
\sigma_t^2 | \mathbf{Z}_t, \hat{y}_{t-1}(\mathbf{S}_t) &\sim IG(\sigma_t^2 | a_t^*, b_t^*), \\
a_t^* &= a_t + n_t/2, \\
b_t^* &= b_t + 0.5 \left(\mathbf{Z}_t^T \tilde{\boldsymbol{\Sigma}}_t^{-1} \mathbf{Z}_t + \boldsymbol{\mu}_{\beta_t}^T \mathbf{V}_{\beta_t}^{-1} \boldsymbol{\mu}_{\beta_t} + \boldsymbol{\mu}_{\boldsymbol{\gamma}_{t-1}}^T \mathbf{V}_{\boldsymbol{\gamma}_{t-1}}^{-1} \boldsymbol{\mu}_{\boldsymbol{\gamma}_{t-1}} - \tilde{\boldsymbol{\mu}}_{\boldsymbol{\beta}_t}^T \tilde{\mathbf{V}}_{\boldsymbol{\beta}_t} \tilde{\boldsymbol{\mu}}_{\boldsymbol{\beta}_t} \right. \\
&\quad \left. - (\mathbf{V}_{\boldsymbol{\gamma}_{t-1}}^{-1} \boldsymbol{\mu}_{\boldsymbol{\gamma}_{t-1}} + \mathbf{g}(\mathbf{S}_t) \hat{y}_{t-1}(\mathbf{S}_t)^T \tilde{\boldsymbol{\Sigma}}_t^{-1} \mathbf{Z}_t)^T \tilde{\mathbf{V}}_{\boldsymbol{\gamma}_{t-1}} (\mathbf{V}_{\boldsymbol{\gamma}_{t-1}}^{-1} \boldsymbol{\mu}_{\boldsymbol{\gamma}_{t-1}} + \mathbf{g}(\mathbf{S}_t) \hat{y}_{t-1}(\mathbf{S}_t)^T \tilde{\boldsymbol{\Sigma}}_t^{-1} \mathbf{Z}_t)\right). \tag{D.3}
\end{aligned}$$

the conditional posterior density function of β_1 is

$$\begin{aligned}\beta_1 | \sigma_1^2, \mathbf{Z}_1 &\sim N(\beta_1 | \tilde{\mathbf{V}}_{\beta_1} \tilde{\boldsymbol{\mu}}_{\beta_1}, \sigma_1^2 \tilde{\mathbf{V}}_{\beta_1}), \\ \tilde{\boldsymbol{\mu}}_{\beta_1} &= \mathbf{V}_{\beta_1}^{-1} \boldsymbol{\mu}_{\beta_1} + \mathbf{h}_1(\mathbf{S}_1) \tilde{\boldsymbol{\Sigma}}_1^{-1} \mathbf{Z}_1, \\ \tilde{\mathbf{V}}_{\beta_1} &= \left(\mathbf{V}_{\beta_1}^{-1} + \mathbf{h}(\mathbf{S}_1) \tilde{\boldsymbol{\Sigma}}_1^{-1} \mathbf{h}(\mathbf{S}_1)^T \right)^{-1},\end{aligned}\tag{D.4}$$

and the marginal posterior density function of σ_1^2 is

$$\begin{aligned}\sigma_1^2 | \mathbf{Z}_1 &\sim IG(\sigma_1^2 | a_1^*, b_1^*), \\ a_1^* &= a_1 + n_1/2, \\ b_1^* &= b_1 + 0.5 \left(\mathbf{Z}_1^T \tilde{\boldsymbol{\Sigma}}_1^{-1} \mathbf{Z}_1 + \boldsymbol{\mu}_{\beta_1}^T \mathbf{V}_{\beta_1}^{-1} \boldsymbol{\mu}_{\beta_1} - \tilde{\boldsymbol{\mu}}_{\beta_1}^T \tilde{\mathbf{V}}_{\beta_1} \tilde{\boldsymbol{\mu}}_{\beta_1} \right).\end{aligned}\tag{D.5}$$